Flow Dynamics and Inclusion Transport in Continuous Casting of Steel

B.G. Thomas, Q. Yuan, L. Zhang, and S.P. Vanka

University of Illinois at Urbana-Champaign
Mechanical and Industrial Engineering.
1206 West Green Street, Urbana, IL 61801
Ph: 217-333-6919, 217-244-4656; Fax: 217-244-6534;
Email: bgthomas@uiuc.edu

ABSTRACT

The quality of continuous cast steel is greatly affected by fluid flow in the mold region, especially involving the transport and entrapment of inclusion particles. As part of a long-term effort to develop and apply comprehensive models of these and other phenomena, this paper reports on work during the first year of this NSF grant to develop quantitative models of transient flow and inclusion transport in the continuous casting of steel, and to apply them to improve understanding and efficiency of inclusion particle removal.

Results are reported here for five interrelated subprojects. Firstly, models of transient flow using Large Eddy Simulation (LES), which were previously validated with digital particle image velocimetry (PIV) measurements in half of a single phase water model of the mold region, are extended to predict asymmetric flow in a full water model and the accompanying transport of inclusion particles. The flow results are validated through comparison with water model measurements and reveal the importance of interaction between the two sides of the caster in producing the large fluctuations. Secondly, the flow model results are used to compute other phenomena of greater influence. Top surface level height is several mm higher towards the narrow faces. Particles are transported according to the local velocities, whose turbulent variations in both time and position lead to asymmetries. Heat transfer in the molten steel pool due to jet impingement requires at least a ½ domain, and a fine mesh to achieve reasonable accuracy. Thirdly, an inclusion size evolution model has been developed for steel melts deoxidized with aluminum. The nucleation of alumina inclusions is very fast and their growth is dominated by turbulent collisions once the particles grow to larger than about 2μm from Ostwald ripening and Brownian motion. Fourthly, an accurate collision probability model has been developed for particle sizes smaller than 40 μm attaching to bubbles. Argon gas bubbles entering the mold are 1-5mm in diameter and greatly increase inclusion removal by attaching with particles. Finally, inclusion entrapment computations compared with measurements in steel product reveal that only a small fraction of the total number of mainly-small inclusions entering the caster appear to be removed, so there is incentive to remove them during upstream processing.

1. INTRODUCTION

Continuous casting produces 96% of the steel manufactured in the U.S. [1] and is the last, and most important, processing step where inclusions can either be generated or removed. Lowering inclusion-related defects is important to improving steel minimum strength, fatigue life, surface appearance, yield and energy efficiency (from reduced rejects), and thereby increase steel industry competitiveness. Moreover, reliable lowering of inclusion entrapment could allow thinner gage products (with associated weight and energy savings) and could reduce the need for costly and energy-intensive secondary refining steps, such as vacuum arc refining and electroslag remelting. Thus, there are tremendous economic, environmental and safety incentives for understanding how to lower the inclusion content of steel.

Plant observations have found that many serious quality problems, including inclusion entrapment, are directly associated with the flow pattern in the mold.[2] Defects caused by nonoptimal fluid flow are even more important to the nearer-net-shape thin-slab casting processes, which are starting to transform the industry.[3] This is because higher velocities are required through a smaller inlet nozzle to cast a thin section slab with the same throughput. Thus, design and control of the fluid flow pattern in the continuous casting mold to minimize inclusions is of crucial importance to the steel industry.

The flow pattern in the mold can be controlled by many variables, including the nozzle and mold geometry, submergence depth, steel flow rate, argon injection rate, electromagnetic stirring, and flux layer properties. Many of these parameters are easy and inexpensive to change and yet have a profound influence on flow and corresponding quality. Currently, flow pattern design is done through trial and error, based on qualitative experiments with water models, plant trials, and the plant operator's experience with defects. Identifying an optimal flow pattern is very difficult, because the fundamental relationship between flow pattern and inclusion entrapment has not been quantified. Thus, each casting operation requires its own expensive experiments, and old defects often reappear when changes in the process occur. With so many different operations and new processes to optimize, the industry can no longer afford this approach.

In previous studies, the principal investigators have applied computational models to increase understanding of flow in the continuous casting mold, using both steady-state[4-21] and transient simulations.[22-29] The reliability of these models to predict flow has been demonstrated through comparison with both water models[9-11, 16, 19, 20, 24, 27, 28] and flow measurements in an operating steel caster.[26, 28] The next step is to apply these models to investigate fundamentally, the associated transport and entrapment of inclusion particles and to determine quantitative relationships between flow pattern control parameters (eg. nozzle geometry) and

2

particle entrapment. The current research is concerned with developing and applying such computations, combined with physical water modeling studies to validate the models and to provide further insight. Finally, plant trials are conducted to further validate the models, and to test proposed improvements. The results of this study should benefit to the steel industry by leading to increased fundamental understanding of inclusion entrapment, and to improvements in design and operating conditions that improve flow pattern in the continuous casting strand and lower costly defects.

2. THE PROCESS

A schematic of part of the continuous casting process is depicted in Figure 1.[30] Steel from the ladle flows through the "tundish," and then it exits down through a ceramic Submerged Entry Nozzle (SEN) and into the mold. Here, the steel freezes against the water-cooled copper walls to form a thin solid shell, which is continuously withdrawn from the bottom of the mold at a "casting speed" that matches the flow of the incoming metal. Flow through the SEN is gravity driven by the pressure difference between the liquid levels of the tundish and the mold top free surfaces. The flow rate is controlled (using feedback from a level sensor) to maintain the liquid level in the mold as constant as possible. In one method, a "stopper rod" extends down through the tundish to partially plug the exit. In another method, a "slide gate" blocks off a portion of the SEN pipe section by moving a disk-shaped plate through a horizontal slit across the entire SEN. Such flow adjustment methods allow for independent control of casting speed and metal level, and are essential for stopping the flow of molten steel if the operation must be abruptly terminated. The submerged nozzle protects the molten steel from exposure to air, which helps to avoid reoxidation and inclusion formation. Together with the casting speed, mold geometry, argon gas injection rate, and other parameters, the nozzle geometry also controls the flow pattern created in the mold cavity. This flow pattern in turn controls the entrapment of inclusions and other defects which determine the steel quality.

3. THE PROBLEM

As shown in Fig. 1, the superheated jet of molten steel from the nozzle traverses across the mold cavity to impinge on the solidifying steel shell near the narrow faces. If the superheat is too large, the flow may break through the shell to create a costly breakout. The jets of molten steel exiting the nozzle also carry particles into the mold cavity in the form of oxide inclusions and argon bubbles, to which inclusions may attach. In addition, high speed flow across the top surface may shear droplets of liquid mold slag into the flow, where they may become entrained in the liquid steel.[31] If the flow pattern enables the particles to

3

reach the top surface, they should be harmlessly removed into the liquid slag layer. However, when the flow pattern is detrimental, particles become entrapped in the solidifying steel shell, where they cause serious quality problems and costly rejects. Particles trapped near the meniscus generate surface delamination defects, and may initiate surface cracks. This occurs when the flow pattern generates excessive surface level fluctuations or insufficient liquid temperatures, so that particles are entrapped by the solidifying meniscus before they can enter the liquid slag. Particles which are entrained into the lower recirculation zones can gradually spiral and become trapped in the solidifying front deep inside the product,[15, 32] leading to internal cracks, slivers in the final rolled product, and blisters.[2] One of these defects, known as "pencil pipes"[31] is caused when small argon gas bubbles surrounded by inclusions are caught in the solidifying shell. During rolling, the inclusion clusters elongate to create long slivers in the final product. During subsequent annealing processes, the trapped bubbles expand to create surface blisters.[31] These intermittent defects are particularly costly because they are often not detected until after many subsequent finishing steps. Thus, there is a great incentive to understand how to control the mold flow pattern in order to minimize particle entrapment and the associated quality problems.

4. PREVIOUS WORK

In work supported by a previous grant, "Study of Transient Flow Structures in the Continuous Casting of Steel", significant advances were made to develop and validate fluid flow modeling tools and to apply them to increase understanding and to improve the continuous casting process. Some of this work is summarized briefly below. More results and details are provided in the more than 30 publications resulting from this project to date [16-21, 24-29, 33-52] and in the website http://ccc.me.uiuc.edu. The flow modeling capability developed in this previous work is being extended to fundamental and practical applications, which are briefly discussed in Section 5 of this paper.

A. Improved models of flow in continuous casting nozzles and mold

Several different computational models have been developed to simulate turbulent fluid flow and heat transfer in continuous casting nozzles and molds, including both large eddy simulations (LES) and conventional time-averaged models, (such as K-ε).[25-27] They have been applied to increase understanding, identify and quantify some of the transient features of the flow field in the continuous casting nozzle, mold, and slag layers, and how they interact. Modeling procedures for obtaining quantitative predictions have been identified. The time-averaged flow pattern predicted from four different methods were compared and found to agree reasonably.[52]   A transient simulation LES1 was computed with a refined Large Eddy

4

Simulation model and the Smagorinsky subgrid scale model, while LES2 used a fine 1.5 million-node grid with no turbulence model (so is really DNS). Time-average results from a conventional K-ε model were similar, although it cannot predict the time-fluctuations properly. Flow field measurements obtained using Particle Image Velocimetry on a scale water mode also matched. [52] Finally, the computational results also compared favorably with velocity measurements in the operating steel caster, [52] using a pair of electromagnetic sensors embedded in the mold wall.[53] Calculations identified how the sensors are reliable only when placed near to the top surface, and when the flow direction is horizontal.[28] All four methods compared are reasonably close for conditions of single phase flow.

The important influence of inlet conditions into the mold on transient flow features was identified using the computational models. Specifically, accurate modeling of the nozzle flow to obtain better inlet conditions was found to change some flow features (such as increasing surface velocities) and better match with the PIV and plant measurements.

B. Benchmark experiments for continuous casting model validation

Experiments were conducted to quantify fluid flow, superheat dissipation, solidifying steel shell growth, heat transfer and microstructure during the continuous casting of stainless-steel slabs at the AK Steel caster in Mansfield, OH.[54] These experimental measurements were further applied to develop, calibrate, and validate mathematical models of both fluid flow and heat flow in continuous casting.[16] Three-dimensional turbulent flow of molten steel in the nozzle and the mold cavity is modeled with the finite difference code CFX 4.2,[55] using the standard K-ε turbulence model and a fixed, structured grid. The results agree with flow measurements in a full-scale water model. The corresponding steady heat conduction equation is solved to predict the distribution of superheat in the molten pool. The predicted temperatures in the molten steel compare well with measurements conducted by inserting a thermocouple probe downward through the top surface at several locations in the operating thin slab caster. Next, solidification of the steel shell is simulated using a transient heat conduction model that features a detailed treatment of the flux layers in the interfacial gap and incorporates the superheat flux calculated from the fluid flow model. This model was calibrated with temperature measurements obtained from thermocouples in the copper mold during operation. It was run under the transient conditions present during a breakout. The predicted shell thickness profiles are compared with many shell thickness profiles measured around the perimeter of a breakout shell. Of greatest interest is the uneven thinning of the shell near the narrow face where the steel jet impinges, which is different between steady-state and the transient conditions of the breakout. This work provides a

set of benchmark experiments for future continuous-casting model development. It further demonstrates the quantitative ability of this modeling approach to simulate coupled fluid flow and solidification heat conduction in a real steel continuous casting process.

C. Nozzle model development and application

Measurements were conducted to validate the ability of flow models to simulate turbulent, multiphase flow through the continuous casting nozzle.[18, 56] The experiments were conducted using particle image velocimetry on 0.4-scale physical water models of the process, using the PIV system at LTV Steel Technical Center. The validated nozzle model has been applied to perform a large, systematic study of the effect of important operating parameters on flow exiting the nozzle.[19, 56] Specifically, the jet characteristics (direction, speed, spread, etc.) exiting the nozzle ports are quantified for different operating parameters (nozzle bore diameter, slide gate orientation, slide gate opening fraction, injected fraction of argon gas, etc.). These results are a necessary first step in determining the important flow pattern in the mold.

D. Nozzle model application: argon gas flow optimization

The validated multiphase flow model of the nozzle was applied to perform over 150 simulations, in order to optimize argon gas injection levels in the nozzle for a range of practical conditions.[56] Specifically, the model results were processed (using simple inverse models) to quantify the minimum argon gas injection levels needed to avoid negative pressure in the nozzle, and thereby avoid air aspiration and the accompanying reoxidation, inclusion formation, and nozzle clogging. Increasing argon gas was found to generally increase nozzle pressure. Some conditions (low tundish level and low casting speed) required very little gas to avoid detrimental air aspiration, while other conditions (deep tundish) required more argon than is practical.[20] The model results can also be used as a clogging index to detect when nozzle clogging is present, before harmful flow defects occur. The implications of these results have been extended in a comprehensive review on how to avoid nozzle clogging.[21]

E. Particle Transport in the Mold

Finally, preliminary studies were performed to predict inclusion transport by extending the LES model of transient flow fields in the mold region. Specifically, Lagrangian particle trajectories were calculated of plastic beads in a water model and compared with measurements of the distribution and flotation removal of the inclusion particles [47]. The LES model was able to reasonably match the measurements both qualitatively and quantitatively. Large particle removal rates were found, (nearly 80%) likely owing to the inability of the smooth walls of the water model to entrap particles. Finally, it was found that large numbers

of particles were required (> 10,000) to obtain reproducible predictions or measurements, owing to the chaotic nature of the particle motion.

5. CURRENT RESULTS

The present paper reports on some recent results from five different components of the current multifaceted research project involving dynamic flow and inclusion transport in the continuous casting mold:

A) asymmetric transient flow

B) surface level, particle transport, and heat transfer in the molten pool

C) nucleation and growth of alumina inclusions in molten steel

D) effect of bubbles on inclusion removal

E) inclusion removal in the steel caster

A. Asymmetric Transient Flow and Particle Transport

Previous computational studies of flow in the continuous casting mold focused exclusively on symmetrical flows. Thus, the first project here investigates asymmetric flow in a full model of the process, consisting of both the complete nozzle (including the stopper rod, submerged entry nozzle and ports) and the mold region. Sample results are presents here from two simulations using the LES approach. First, the flow in a full-scale water model was simulated and compared with measurements. Then a simulation of the turbulent flow and inclusion transport in the corresponding full-scale steel caster is performed. The conditions were chosen to match conditions at the AK Mansfield thin slab caster documented elsewhere [16, 54] where plant measurements were already available (132 x 984mm section, 1 m/min, 59 ^{0}C superheat).

The flow in the complex shaped nozzle is computed using LES (with approx. 630,000 cells), and the exit velocities were stored every 0.025 seconds for a period of 9.45 seconds. These were then used as inlet values to the two mold flow simulations, and recycled periodically. This two-step procedure greatly improved stability of the computation, while lowering the memory needed for a given simulation to less than 1.5 GB, (memory currently limits the problem size).

The time-dependent three-dimensional Navier-Stokes equations were solved using the Harlow-Welch fraction step procedure. Second order central differencing is used for the convection terms and the Crank-

Nicolson scheme is used for the diffusion terms. The Adams-Bashforth scheme is used to discretize in time with second order accuracy. The pressure Poisson equation is solved using an Algebraic Multi-grid solver. No sub-grid model was used, while a dynamic model for the sub-grid scale kinetic energy has been developed for the use of continuing simulations. Computational grids consisting of 0.7 million and 1.3 million cells are used for these two mold region computations.

The water model differs from the real steel caster in several respects important to fluid flow. First, the side walls of the water model, which represent the moving solidifying shell, are non-porous and stationary. Further, the water model has a flat bottom with outlet ports to represent the tapering molten pool of a curved casting machine. Figure 2 shows the computational domain of the steel caster, which includes these effects. Special source terms were added for both mass and momentum in order to satisfy the conditions on the moving boundaries of the domain, which represent the dendritic solidification front.

Figures 3 and 4 present typical instantaneous and time-averaged (over 22 seconds) velocity vector plots at the centerplane of the steel casting machine This particular nozzle geometry features an additional central downward jet entering the mold, in addition to the classic bifurcated nozzle ports sending fluid toward the narrow faces. The turbulent structures in the mold and a slight asymmetry between the two side jets can be seen in this instantaneous plot. The time-averaged plot shows a double-roll flow pattern on each side. Qualitatively similar flow patterns are also seen in the water model simulation.

Figure 5 compares LES with the dye injection measurement in the water model. The solid line shows the flow speed along the jet centerline obtained from LES average data. The dark dots present the measured speed. A reasonable agreement is seen between LES and the measurements.

The difference between water models and real steel casting machines is investigated in Figures 5 and 6, which compare the time-averaged downwards flow velocity (and its rms) of the water model and casting machine along a horizontal line 1000mm below the meniscus and 164mm from the narrow face. The data are time averaged over 48s and 22s for the water model and casting machine respectively. Figure 5 shows a bigger spatial variation of the downwards velocity for the water model. It also shows that the steel caster has less upward (ie "reverse") flow. Two main reasons are suspected to cause this: the tapering and solidification restricts the flow domain, which makes the flow easier to get evenly distributed; and the downwards withdrawing of the shells prevents the flow from having upwards velocities. An asymmetry

8

between the two sides can also be seen for both the water model and casting machine, implying that a low frequency oscillation between the two sides exists and 48 seconds are not enough for the time average.

Figure 7 shows the time-variation of the horizontal velocity towards the SEN at the center points between the SEN and the narrow faces on the meniscus, obtained from the steel caster simulation. This figure shows a large transient component, which is observed in water models, but was not observed in half-caster simulations (which assumed symmetrical flow in each half). This suggests that interaction between the two sides of the caster is the cause the large fluctuations. The variations are significant, because the level fluctuations which accompany them are the major cause of defects in the process.

B. Surface Level, Particle Transport, and Heat Transfer in the Molten Pool

Having been validated, the flow model is next applied to investigate related phenomena. Although a critical first step, the flow field is not the primary interest of this project. Defects in the process are generated by the phenomena which accompany the dynamic flow field. These include motion of the top surface level, transport of inclusion particles, and heat transfer. Each of these is discussed in turn:

i). Top Surface Level

Figure 8 shows an example of the instantaneous variation in surface level predicted from the pressure output from the LES flow model. The level is always higher near the narrow faces, by 4-6mm. This is because the steel momentum up the narrow faces lifts the liquid level there, displacing some of the molten flux. The flux layer must be thick enough to cover the steel, in order to provide a steady supply of molten flux into the interfacial gap to lubricate the steel. Insufficient flux consumption leads to temperature fluctuations which cause surface cracks and other defects in the solid steel product. Thus, the height of the surface "standing wave" is important to steel quality. The predictions here compare reasonably with industry measurements using nail boards and sheets.

ii) Particle Transport and Entrapment

Another important consequence of the flow pattern in the mold is the transport of inclusion particles within the molten pool. Inclusions may eventually be removed harmlessly into the top slag layer, or they may become entrapped in the solidifying shell. Fundamental criteria have been developed for the capture of inclusions by a moving dendritic interface through engulfment or entrapment, considering together for the first time: critical interface velocity, particle size, and local cross-flow velocity. Small inclusions (<40 μm)

9

are predicted to become surrounded by the dendrite arms and entrapped with little chance of "particle pushing". Figure 9 shows the particle distribution and entrapment locations at three instants for the mold and flow conditions just discussed, for such small inclusions.

Particles are seen to move with the jet and reach the walls 0.6 seconds after injection at 33s. The particles split into two groups by 2 seconds (second frame) and enter the upper and lower rolls. Although the flow and distribution exiting the nozzle is initially almost symmetrical, a significant asymmetry can be seen to develop in the 15 s plot, indicating the important effects of flow asymmetry on particle transport. It is important to note that the inlet velocity distribution was relatively uniform during this time, so the asymmetry in this case is caused solely by chaotic turbulent motion below the mold. The downward motion corresponds to large asymmetry between the velocities at these 2 points, showing that particle motion is dominated by the flow distribution, regardless of particle size. The velocities are seen in Figure 10 to fluctuate, indicating that particles injected at other times will show the opposite asymmetry or behave almost the same. These results are important because particles which are transported deeper are more likely to become permanently entrapped in the steel caster.

iii) Heat Transfer in the Molten Steel Pool

Large eddy simulations were next carried out to study transient fluid flow and turbulent heat transfer in this thin slab caster. Previous simulations of turbulent heat transfer in unconstrained circular impinging jets revealed that very fine meshes are needed near the impingement plate to predict the heat transfer rate correctly in LES simulations [26]. Heat transfer simulations require higher grid density than flow simulations.

Two simulations of a real steel caster have been carried out. First a ¼ mold simulation was performed with 0.8 million finite volume cells, assuming symmetrical boundary conditions on the two vertical center-planes of the simulation domain. This produced results which did not match the water model, or the full-mold simulations. The imposed WF-WF symmetry condition severely constrained the jet coming out from the side port so that it had too much diffusion in the vertical direction. Consequentlly, there was quiescent flow in the top region, with no upper recirculation zone in the flow field. This incorrect flow field produces a weak jet impingement that gives a lower heat transfer rate on the NF, and allows the upper corner region to freeze. Thus, the application of two-fold WF-WF symmetry is inappropriate for transient LES simulations.

The ½ mold simulation (1.6 million finite volume cells) addresses this problem and shows good tendency towards a correct solution. Figure 11 shows an instantaneous snapshot of the velocity and temperature fields in the ½ mold simulation. The flow field compares reasonably well with the dye-injection experiment and full-mold computations presented in section 5A.

C. Nucleation and Growth of Alumina Inclusions in Molten Steel

Inclusion distribution computations require knowledge of the size distribution of particles entering the caster. The size distribution may be important to inclusion entrapment, and the size of captured inclusions is crucial to final steel quality, as defects increase with the size of non-metallic inclusion clusters. Previous work has used measured size distributions as the initial condition [35]. As part of this project, a fundamental model has been developed to predict the size distribution of indigineous inclusions in low carbon steels deoxidized with aluminum.

Inclusions arise from many sources, including deoxidation, reoxidation, slag entrapment, chemical reactions, and exogenous inclusions. Inclusion evolution and removal is affected by diverse complex phenomena, including deoxidant quantity, composition, and morphology, vessel geometry, transport by turbulent flow, interfacial tension, diffusion coefficient, the initial oxygen content, collisions with both bubbles and other particles, reoxidation, temperature, and properties of the slag layer and vessel walls where inclusions may be removed or generated. A common characteristic of indigenous alumina inclusions in Low Carbon Al-Killed (LCAK) steel [57-70] is that the central globule, secondary dendrite arms, or the individual spherical inclusions in an inclusion cluster is consistently 1~4 μm (Fig. 12).

A computational model based on classic homogenous nucleation theory, thermodynamic analysis and numerical simulation, has been developed to predict of the nucleation and growth of the alumina size distribution in the molten steel, including the effects of Ostwald ripening, Brownian collision and turbulent collision. The model was tested by applying it to aluminum deoxidation of a typical steel-oxygen system, where previous measurements and calculations were available. The vessel was a 50 tonne ladle of low-carbon steel refined in an ASEA-SKF furnace.[71] The total oxygen before adding aluminum is around 300 ppm and the final free oxygen is about 3 ppm, which corresponds to a 46kg aluminum addition. The delay constant K was assumed to be 0.1. [72] The ladle had 2.3m diameter and 1.7m depth, which corresponds to a turbulent energy dissipation rate in the melt of 0.01224 m^2/s^3 (856.8 erg/cm^3s).

Starting with rapid supersaturation with Al_2O_3 "pseudo-molecules", homogeneous nucleation is very fast, occurring mainly between 1μs and 10μs. The stable inclusion nuclei are predicted to be only about 10-20 Å in diameter. The growth of inclusions smaller than 1μm in radii is mainly controlled by diffusion of pseudo-molecules and Brownian collision, and inclusions in this range tend to be spherical. The growth of inclusions larger than 2μm in radii is mainly controlled by turbulent collisions, and inclusions in this range tend to form clusters which retain minimum feature sizes of 1~2μm.

Figure 13 shows a histogram of inclusion size distribution at different times after adding aluminum to the ladle, assuming that all inclusions with radii larger than 36μm are instantly removed to the top slag. Inclusion size distribution can reach 0.1~1μm at 6s and 0.1~36μm at 100s, which agrees roughly with the industrial measurements [73, 74] After 720 seconds, total oxygen in the steel decreases to around 20 ppm, which agrees with other measurements. [71]

In addition to providing needed input conditions for the mold inclusion calculations, this deoxidation model also reveals important insights into optimal steel refining practice. The effect of stirring power on the oxygen removal rate constant in different steel refining vessels is shown in Fig. 14 [75, 76]. Excessive stirring is detrimental as the upward circulation of steel onto the slag layer may expose an "eye" region of the steel surface to reoxidation and the lining may be seriously eroded. The calculated effect of stirring power on inclusion size distribution, shown in Fig. 15, indicate that increasing stirring power generates more large inclusions in the bulk. If these inclusions can be removed into the slag, this improves cleanliness. This is very bad for steel cleanliness, however, if the stirring power is high at the end of refining, when the new large inclusions have no time to be removed. Therefore, the recommended practice is to first stir vigorously, to encourage the collision of small inclusions into large ones, followed by a "final stir" that slowly recirculates the steel to facilitate their removal into the slag while minimizing the generation of more large inclusions via collisions.

D.   Interaction between inclusions and bubbles in liquid steel

Inclusion removal from molten steel is greatly assisted by gas injection, which is also used to promote homogeneity in temperature and composition. Argon injection into the Submerged Entry Nozzle (SEN) of continuous casting is very common, and also has a large effect on the mold flow pattern. Thus, fundamental models of the interaction between alumina inclusions and argon bubbles in steel are being developed. Figure

16 shows the terminal velocities of gas bubbles in liquid steel based on different models. [73, 77-83] The agreement among these models is very rough, so a mean relationship between bubble velocity and size is adopted. A peak rising velocity can be seen at a bubble diameter of 1-3 mm. In the regime smaller than 1 mm, the bubbles are spherical [82]. When the equivalent bubble diameter exceeds 3 mm, the bubble shape becomes ellipsoidal and then spherical caps. Beyond 7 mm, the bubble velocity gradually increases again.

The attachment of inclusions to bubbles is characterized by their collision probability, which is defined as the fraction of inclusions in the path of the bubble that actually collide with it and attach, P_c. Inclusions within area $\pi d_b^2/4$ attach to the bubble surface with probability P_c, as illustrated in Fig. 17. An upper limit, based on streamline potential flow, depends on the ratio of the area (S_{OC}) inscribed by the limiting diameter (d_{OC}) to the area (S_B) inscribed by the bubble diameter (d_B).

$$P_C = \frac{S_{oc}}{S_B} = \left(\frac{d_{oc}}{d_B}\right)^2 \tag{1}$$

This theory assumes that the particle attaches to the bubble if its trajectory, assumed to follow the fluid streamlines around the bubble, takes it within its radius of the bubble surface. Simulations were performed to improve on this simple theory by incorporating inertial effects, due to the density difference between particle and fluid. Alumina inclusions in steel with argon bubbles corresponds to the case of 2800 kg/m3 in Fig. 18, where the lighter particle is diverted further around the bubble, thus lowering its attachment probability, relative to heavy particles in water.

For validation purposes, model predictions using FLUENT are compared in Fig. 19 with experiments in water measuring silica particle attachment probability to 1.52mm diameter air bubbles rising at 0.315 m/s. Agreement is good for small particles ($< 40\mu m$). This figure also validates the numerical formulation and choice of parameters such as mesh and time step size, because the probability computation for zero-drag neutral-density-particles matches the analytical solution. Fig. 19 also shows the importance of using the correct zero shear stress boundary condition at the bubble / fluid interface. Small particles are seen to have a higher collision probability with bubbles than with large solid particles, which have a no slip interface condition.

13

Having been validated, the FLUENT model is next used to calculate collision probabilities between argon bubbles and small inclusions in molten steel. Figure 20 shows sample results, which indicate that smaller bubbles are more favorable for inclusion removal by bubble flotation (for a given gas fraction). However, the small bubbles at least have the following two shortcomings: 1).Smaller bubbles require longer rising time. In practice, shorter treatment times will significantly reduce operational costs by reducing the temperature loss and refractory consumption; 2). Small bubbles (<1mm) are much more easily trapped in the recirculation zone of the bulk or re-entrained into bulk from the interface between liquid steel and slag and some of then finally are captured in the solidified front. Previous work [84], shows that the horizontal velocity of liquid steel near the free surface of the continuous casting mold is about 0.11~0.25m/s, and in a ladle system is about 0.1m/s [85]. The bubble rising velocity should be greater than this to avoid re-entrainment, which suggests the bubble size should be greater than 1mm.

Gas can be injected into liquid steel by various means, such as tuyere, lance, and porous refractory plugs. In addition to its dependence on the gas flow rate, the bubble size decreases with stirring intensity in the liquid (figure 21) [86]. If a gas bubble exceeds a critical maximum size d_{Bmax}, it will be broken up. Thus, higher stirring intensity favors the generation of smaller bubbles. The stirring intensities of various metallurgical systems are compared in the ranges included at the top of Fig. 21. The highly turbulent flow inside a submerged entry nozzle (SEN) [84] is predicted to break apart bubbles larger than about 5 mm in diameter. Assuming similar conditions exist in the ladle to tundish shroud, injected gas should break up into bubbles that are sufficiently small to collect particles, while also being sufficiently large to float to the free surface of the tundish. Thus, if gas injection rate is kept small enough to avoid excessive surface disruption, the ladle to tundish is a good place to inject gas to remove the inclusion by bubble flotation. This location minimizes the danger of small bubbles becoming entrapped in the solidifying steel shell, which is always a danger of bubble injection into the mold or SEN.

E.   Inclusion Removal in the Steel Caster

Although a very powerful approach, it is not feasible to apply fine-grid LES simulations to perform large parametric studies over the many real process design variables that are important. Thus, another subproject was initiated to find more computationally efficient methods to predict inclusion particle distributions. To benchmark the accuracy of the methods, the computations are compared with both LES simulations and

plant experiments. Here, steady flow in the continuous caster is simulated with the standard k-ε two-equation turbulence model. Each inclusion trajectory is calculated by integrating its local velocity, considering its drag and buoyancy forces. A "random walk" model is used to incorporate the effect of turbulent fluctuations on the particle motion. In this model, the particle moves within local turbulent eddies over the eddy lifetime. The local velocity fluctuation is based on a Gaussian-distributed random number, chosen according to the local turbulent kinetic energy, K. The random number is changed, thus producing a new instantaneous velocity fluctuation, with a frequency equal to the characteristic lifetime of the eddy.

The inclusion entrapment model is being tested through comparison with plant experiments. The casting conditions are given in Table I. Inclusion size distributions were measured using "slime extraction", whereby several hundred samples over many steel heats, each consisting of several hundred grams, were dissolved to extract the inclusions. The inclusions were suspended in water and their size distributions measured with a Coulter counter. Results are given in Fig. 22, which show that most of the inclusion mass is between 10-30 μm. Although rare, the inclusions larger than 50μm are very detrimental to steel quality, and can only be detected with large sample sizes. Thus, total oxygen measurements are less reliable means to quantify inclusion size distributions. Figure 23 shows the inclusion size distribution measured through the slab thickness, indicating that more inclusions are found near the surfaces.

Table I Simulation parameters for Steel Caster

	Experiment
Nozzle port size/Inlet port size (x×y) (m)	0.065×0.080
Nozzle angle	15°
Submergence depth (m)	0.30
Mold/Domain geometry specification	Open bottom
Mold/Domain height (m)	**2.55**
Mold/Domain width (m)	1.3
Mold/Domain thickness (m)	0.25
Average inlet flow rate (m^3/s)	0.00325
Casting speed (m/min)	1.2
Fluid density (kg/m^3)	**7020**
Fluid kinetic viscosity (m^2/s)	**$0.954×10^{-6}$**
Particle size (diameter) ((μm)	**0.5-300**
Particle density (kg/m^3)	5000
Turbulence model	k-ε
Inclusion motion model	Random walk, 0.1s time step, 10000-15000 inclusion injected.
Boundary condition to the Inclusions	Escape from top surface and open

	bottom; at wide faces and narrow faces, inclusion will be trapped when they touch them.
Inlet condition for fluid flow	Simulation of nozzle outlet port
Gas flow rate	None

The results tabulated in Table II, compare the inclusion fractions entrapped at different destinations with the industrial measurements. Figure 24 shows the entrapped positions on the wide face of 50 μm simulated inclusions. For inclusions smaller than 50 μm, only 7% are safely removed by the top surface, independent of inclusion size. A larger fraction of inclusions bigger than 50 μm are removed.

The majority of inclusions (65%) are captured within 28mm of the surface, which represents the top 2.55m of the caster. This agrees only qualitatively with the measurements in Fig. 23. A disproportionately large fraction of these (24%) are captured in the narrow face, despite its smaller surface area, owing to the jet impingement against its inner solidification front. Inclusions exiting the domain are entrapped somewhere deeper than 28mm. If the entrapment criteria are the same for small and large inclusions, their entrapment to walls are very similar at 0-28mm slab surface thickness. Only 7-12% of the inclusions are predicted to be removed by the top surface, compared with a measured total inclusion volume fraction removal to top surface of 20%. Thus, the current entrapment model at the walls underpredicts inclusion removal. This is likely due in part to the neglect of interaction with argon bubbles in the present computation. Further work is needed to validate this model with the LES model predictions, and to refine the model to obtain better quantitative match with experiments, prior to performing parametric studies.

Table II. Inclusions fractions entrapped at different positions in the caster

Inclusion size	Wide face		Narrow face		28-125mm	Top
	0-15mm	15-28mm	0-15mm	15-28mm		
50mm	27%	15%	15%	10%	28%	7%
225mm	29%	12%	14%	10%	23%	12%
Industrial Measurement						20%

6. SIGNIFICANT FINDINGS

Advanced computational models are being developed to predict quantitatively, the removal of inclusions in the mold region during the continuous casting steel. This multi-faceted research project includes models of transient fluid flow in the nozzle and mold, fluctuation of the top free surface, and the transport of heat and inclusion particles. The final system of models will incorporate the results of other models, including: 1) nucleation and growth to find the inclusion size distributions, 2) argon bubble size distribution, relative rising velocity, and inclusion attachment probability, and 3) entrapment criteria at the solidification front and top surface. Each aspect of the models is being tested through extensive comparison with measurements, including the measurement of total inclusion entrapment in the cast steel product at the plant. This work has already obtained several findings, which are very significant to the accurate prediction of inclusion behavior in continuous casting.

1) The interaction between the left and right sides of the caster produces asymmetric flow, which is significant both at the top surface (influencing velocity fluctuations and standing wave), and in the lower recirculation zone (influencing entrapment to the shell).

2) Particle transport is governed by the fluid flow pattern, leading to asymmetric entrapment profiles.

3) Nucleation of alumina inclusions is very fast and growth is dominated by turbulent collisions once the particles grow to larger than about 2μm from Ostwald ripening and Brownian motion.

4) Argon gas bubbles are 1-5mm in size and greatly increase inclusion removal by attaching to particles. Solid particles attaching to air bubbles in water behave differently than alumina particles attaching to argon bubbles in molten steel, so computational models are needed.

5) Finally, inclusion particle entrapment locations are predicted and compared with measurements in the final product: only a small fraction of the total inclusions entering the caster (which are mainly smaller than 30μm) appear to be removed, so there is great incentive to remove them during upstream processing. The removal of larger inclusions is more difficult both to measure and to compute, but is the focus of continuing efforts, owing to its greater importance to steel quality.

7. IMPACT

This work aims to improve understanding of transient flow, inclusion transport and defect formation in the mold region during the continuous casting of steel slabs, through the development, validation, and application of fundamental computational models of transient fluid flow. Plant observations have found that many serious quality problems, including inclusion entrapment, are directly associated with the flow pattern in the mold. The results from the computational simulations of this work are increasing fundamental understanding of transient fluid flow, gas, and inclusion particle transport in the mold region. This will lead to optimized nozzle geometry and gas flow rates to improve mold flow patterns and minimize inclusion defects. Lowering defects from internal inclusions can improve steel minimum strength, fatigue life, surface appearance, yield and energy efficiency (from reduced rejects) and lower production cost. Furthermore, the computational tools developed and validated in this work can be applied to study and optimize flow in other processes.

8. ACKNOWLEDGMENTS

9. REFERENCES

1. "Continuously Cast Steel Output, 1999," Report, International Iron Steel Institute, Brussels, Belgium, 2000, www.worldsteel.org.

2. J. Herbertson, Q.L. He, P.J. Flint, R.B. Mahapatra, "Modelling of Metal Delivery to Continuous Casting Moulds," in Steelmaking Conf. Proceedings, Vol. 74, ISS, Warrendale, PA, 1991, 171-185.

3. T. Honeyands and J. Herbertson, "Oscillations in Thin Slab Caster Mold Flows," 127th ISIJ Meeting, ISIJ, Tokyo, Japan, 1994.

4. B.G. Thomas, "Application of Mathematical Models to the Contious Slab Casting Mold.," ISS Trans., Vol. 16 (12), 1989, 53-66.

5. B.G. Thomas, "Mathematical Modeling of the Continuous Slab Casting Mold, a State of the Art Review," in Mold Operation for Quality and Productivity, A. Cramb, ed. Iron and Steel Society, Warrendale, PA, 1991, 69-82.

6. B.G. Thomas and F.M. Najjar, "Finite-Element Modeling of Turbulent Fluid Flow and Heat Transfer in Continuous Casting," Applied Mathematical Modeling, Vol. 15 (5), 1991, 226-243.

7. X. Huang, B.G. Thomas and F.M. Najjar, "Modeling Superheat Removal during Continuous Casting of Steel Slabs," Metall. Trans. B, Vol. 23B (6), 1992, 339-356.

8. X. Huang and B.G. Thomas, "Modeling of Steel Grade Transition in Continuous Slab Casting Processes," Metall. Trans., Vol. 24B (2), 1993, 379-393.

9. D.E. Hershey, B.G. Thomas and F.M. Najjar, "Turbulent Flow through Bifurcated Nozzles," Int. J. Num. Meth. in Fluids, Vol. 17 (1), 1993, 23-47.

10. B.G. Thomas and X. Huang, "Effect of Argon Gas on Fluid Flow in a Continuous Slab Casting Mold," 76th Steelmaking Conference Proceedings, (Dallas, TX), Iron and Steel Society, Warrendale, PA, Vol. 76, 1993, 273-289.

11. B.G. Thomas, X. Huang and R.C. Sussman, "Simulation of Argon Gas Flow Effects in a Continuous Slab Caster," Metall. Trans. B, Vol. 25B (4), 1994, 527-547.

12. G.D. Lawson, S.C. Sander, W.H. Emling, A. Moitra, B.G. Thomas, "Prevention of Shell Thinning Breakouts Associated with Widening Width Changes," in Steelmaking Conference Proceedings, Vol. 77, Iron and Steel Society, (Warrendale, PA), 1994, 329-336.

13. F.M. Najjar, B.G. Thomas and D.E. Hershey, "Turbulent Flow Simulations in Bifurcated Nozzles: Effects of Design and Casting Operation," Metall. Trans. B, Vol. 26B (4), 1995, 749-765.

14. R. McDavid and B.G. Thomas, "Flow and Thermal Behavior of the Top-Surface Flux/ Powder Layers in Continuous Casting Molds," Metall. Trans. B, Vol. 27B (4), 1996, 672-685.

15. B.G. Thomas, A. Denissov and H. Bai, "Behavior of Argon Bubbles during Continuous Casting of Steel," in Steelmaking Conference Proceedings, Vol. 80, ISS, Warrendale, PA., 1997, 375-384.

16. B.G. Thomas, R. O'Malley, T. Shi, Y. Meng, D. Creech, D. Stone, "Validation of Fluid Flow and Solidification Simulation of a Continuous Thin Slab Caster," in Modeling of Casting, Welding, and Advanced Solidification Processes, Vol. IX, Shaker Verlag GmbH, Aachen, Germany, (Aachen, Germany, August 20-25, 2000), 2000, 769-776.

17. H. Bai and B.G. Thomas, "Bubble Formation during Horizontal Gas Injection into Downward Flowing Liquid," Metall. Mater. Trans. B, 2001, under review.

18. H. Bai and B.G. Thomas, "Turbulent Flow of Liquid Steel and Argon Bubbles in Slide-Gate Tundish Nozzles, Part I, Model Development and Validation," Metall. Mater. Trans. B, Vol. 32B (2), 2001, 253-267.

19. H. Bai and B.G. Thomas, "Turbulent Flow of Liquid Steel and Argon Bubbles in Slide-Gate Tundish Nozzles, Part II, Effect of Operation Conditions and Nozzle Design," Metall. Mater. Trans. B, Vol. 32B (2), 2001, 269-284.

20.   H. Bai and B.G. Thomas, "Effects of Clogging, Argon Injection and Continuous Casting Conditions on Flow and Air Aspiration in Submerged Entry Nozzles," Metall. Mater. Trans. B, 2001, in press.

21.   B.G. Thomas and H. Bai, "Tundish Nozzle Clogging – Application of Computational Models," in Steelmaking Conf. Proc., Vol. 18, Iron and Steel Society, Warrendale, PA, 2001, 895-912.

22.   B.G. Thomas, "Modeling Study of Intermixing in Tundish and Strand during a Continuous-Casting Grade Transition," Iron and Steelmaker, Vol. 24 (12), 1997, 83-96.

23.   X. Huang and B.G. Thomas, "Modeling of Transient Flow Phenomena in Continuous Casting of Steel," Canadian Metall. Quart., Vol. 37 (304), 1998, 197-212.

24.   B.G. Thomas, H. Bai, S. Sivaramakrishnan, S.P. Vanka, "Detailed Simulation of Flow in Continuous Casting of Steel Using K-e, LES, and PIV," International Symposium on Cutting Edge of Computer Simulation of Solidification and Processes, (Osaka, Japan, Nov. 14-16, 1999), ISIJ, 1999, 113-128.

25.   B.G. Thomas and S.P. Vanka, "Study of Transient Flow Structures in the Continuous Casting of Steel," NSF Design & Manufacturing Grantees Conference, (Long Beach, CA), NSF, Washington, D.C., 1999.

26.   B.G. Thomas and S.P. Vanka, "Study of Transient Flow Structures in the Continuous Casting of Steel," NSF Design & Manufacturing Grantees Conference, (Vancouver, Canada), NSF, Washington, D.C., 2000, 14p.

27.   B.G. Thomas and S.P. Vanka, "Study of Transient Flow Structures in the Continuous Casting of Steel," NSF Design & Manufacturing Grantees Conference, (Jan. 7-10, Tampa, FL), NSF, Washington, D.C., 2001, 14p.

28.   S. Sivaramakrishnan, H. Bai, B.G. Thomas, P. Vanka, P. Dauby, M. Assar, "Transient Flow Structures in Continuous Cast Steel," in Ironmaking Conference Proceedings, Vol. 59, ISS, Warrendale, PA, (Pittsburgh, PA), 2000, 541-557.

29.   S. Sivaramakrishnan, B.G. Thomas and S.P. Vanka, "Large Eddy Simulation of Turbulent Flow in Continuous Casting of Steel," in Materials Processing in the Computer Age, Vol. 3, V. Voller and H. Henein, eds., TMS, Warrendale, PA, 2000, 189-198.

30.   B.G. Thomas, "Modeling of the Continuous Casting of Steel: Past, Present, and Future, Dr. J. Keith Brimacombe Lecture," in Electric Furnace Conf. Proc., Vol. 59, ISS, Warrendale, PA, (Phoenix, AZ), 2001, 3-30.

31.   W.H. Emling, T.A. Waugaman, S.L. Feldbauer, A.W. Cramb, "Subsurface Mold Slag Entrainment in Ultra-Low Carbon Steels," in Steelmaking Conference Proceedings, Vol. 77, ISS, Warrendale, PA, (Chicago, IL), 1994, 371-379.

32.   R.C. Sussman, M. Burns, X. Huang, B.G. Thomas, "Inclusion Particle Behavior in a Continuous Slab Casting Mold," in 10th Process Technology Conference Proc., Vol. 10, Iron and Steel Society, Warrendale, PA, (Toronto, Canada, April 5-8, 1992), 1992, 291-304.

33. B.G. Thomas, "Mathematical Models of Continuous Casting of Steel Slabs," Report, Continuous Casting Consortium, University of Illinois at Urbana-Champaign, 1999.

34. B.G. Thomas, "University - Steel Industry Interaction, R&D in the Steel Industry," 40th Congreso Latinoamericano de Siderurgia, ILAFA 40 Congress Proceedings, (Buenos Aires, Argentina), Inst. Argentino de Siderurgia, 1999, 65-67.

35. Y. Miki and B.G. Thomas, "Modeling of Inclusion Removal in a Tundish," Metall. Mater. Trans. B, Vol. 30B (4), 1999, 639-654.

36. B.G. Thomas, "Mathematical Models of Continuous Casting of Steel Slabs," Report, Continuous Casting Consortium, University of Illinois at Urbana-Champaign, 2000.

37. B.G. Thomas, "The Importance of Numercial Simulations for Further Improvements of the Continuous casting Process," 8th International Continuous Casting Conference, (Linz, Austria, August 20-25, 2000), Voest Alpine, Linz, Austria, 2000, 7.1-7.11.

38. H. Bai and B.G. Thomas, "Effect of Clogging, Argon Injection, and Casting Conditions on Flow Rate and Air Aspiration in Submerged Entry Nozzles Steel," in 83rd Steelmaking Conference Proceedings, Vol. 83, ISS, Warrendale, PA, (Pittsburgh, PA, March 2-29, 2000), 2000, 183-197.

39. H. Bai and B.G. Thomas, "Two-Phase Flow in Tundish Nozzles During Continuous Casting of Steel," in Materials Processing in the Computer Age, Vol. 3, V. Voller and H. Henein, eds., TMS, Warrendale, PA, 2000, 85-99.

40. B.G. Thomas, "Continuous Casting," in The Encyclopedia of Materials: Science and Technology, Vol. 2, D. Apelian, ed. Elsevier Science Ltd., Oxford, UK., 2001, 6p.

41. B.G. Thomas, "Fundamentals of Continuous Casting: Modeling," in Making, Shaping and Treating of Steel: Continuous Casting, Vol. 5, A. Cramb, ed. AISE Steel Foundation, Pittsburgh, PA, 2001, Chapter 3.9, submitted Oct., 2000.

42. B.G. Thomas, "Continuous Casting Operation: Fluid Flow," in Making, Shaping and Treating of Steel: Continuous Casting, Vol. 5, A. Cramb, ed. AISE Steel Foundation, Pittsburgh, PA, 2001, Chapter 4.3, submitted Oct., 2000.

43. B.G. Thomas, "Continuous Casting of Steel, Chap. 15," in Modeling and Simulation for Casting and Solidification: Theory and Applications, O. Yu, ed. Marcel Dekker, New York, 2001, in press.

44. T. Shi and B.G. Thomas, "Effect of Gas Bubble Size on Fluid Flow in Continuous Casting Mold," Report, Continuous Casting Consortium, 2001.

45. Q. Yuan, S.P. Vanka and B.G. Thomas, "Large Eddy Simulations of Turbulent Flow and Inclusion Transport in Continuous Casting of Steel," 2nd International Symposium on Turbulent and Shear Flow Phenomena, June 27 - 29, 2001, Royal Insitute of Technology(KTH), Stockholm, Sweden, 2001, 6.

46.   C. Bernhard, B.G. Thomas, G. Xia, C. Chimani, "Simulation of Solidification and Microstructure in Continuous Casting," Berg- und Huettenmaennische Monatshefte, 2001, submitted, June, 2001.

47.   Q. Yuan, S.P. Vanka and B.G. Thomas, "Large Eddy Simulations of Turbulent Flow and Inclusion Transport in Continuous Casting of Steel," 2nd International Symposium on Turbulent and Shear Flow Phenomena, June 27 - 29, 2001, Royal Institute of Technology (KTH), Stockholm, Sweden, Vol. 2, 2001, 519-524.

48.   Q. Yuan, T. Shi, B.G. Thomas, S.P. Vanka, "Simulation of Fluid Flow in the Continuous Casting of Steel," Computational Modeling of Materials, Minerals and Metals Processing, (Seattle, CA, Feb. 18-20, 2002), TMS, Warrendale, PA, 2001, 491-500.

49.   B.G. Thomas, "Continuous Casting: Complex Models," in The Encyclopedia of Materials: Science and Technology, Vol. 2, K.H. J. Buschow, R. Cahn, M. Flemings, B. Ilschner, E. J. Kramer, S. Mahajan and s.e. J. Dantzig, eds., Elsevier Science Ltd., Oxford, UK, 2001, 1599-1609.

50.   B.G. Thomas and L. Zhang, "Mathematical Modeling of Fluid Flow in Continuous Casting: a Review," ISIJ Internat., Vol. 41 (10), 2001, 1185-1197.

51.   B.G. Thomas, Q. Yuan, S. Sivaramakrishnan, T. Shi, S.P. Vanka, M.B. Assar, "Comparison of Four Methods to Evaluate Fluid Velocities in a Continuous Casting Mold," ISIJ Internat., Vol. 41 (10), 2001, 1266-1276.

52.   B.G. Thomas, Q. Yuan, S. Sivaramakrishnan, T. Shi, S.P. Vanka, M.B. Assar, "Comparison of Four Methods to Evaluate Fluid Velocities in a Continuous Casting Mold," ISIJ Int., Vol. 41 (10), 2001, 1262-1272.

53.   P. Andrzejewski, D. Gotthelf, E. Julius, H. Haubrich, "Mould Flow Monitoring at No. 3 Slab Caster, Krupp Hoesch Stahl AG," in Steelmaking Conference Proceedings, Vol. 80, ISS, Warrendale, PA, 1997, (Chicago, IL), 1997, 153-157.

54.   B.G. Thomas, R.J. O'Malley and D.T. Stone, "Measurement of temperature, solidification, and microstructure in a continuous cast thin slab," Modeling of Casting, Welding, and Advanced Solidification Processes, (San Diego, CA), TMS, Warrendale, PA, Vol. VIII, 1998, 1185-1199.

55.   CFX 4.2, Report, AEA Technology, 1700 N. Highland Rd., Suite 400, Pittsburgh, PA 15241, 1998.

56.   H. Bai, "Argon Bubble Behavior in Slide-Gate Tundish Nozzles During Continuous Casting of Steel Slabs," PhD Thesis, University of Illinois, 2000.

57.   E.T. Turkdogan, "Deoxidation of Steel," JISI, 1972, 21-36.

58.   R.A. Rege, E.S. Szekeres and W.D. Forgeng, "Three-Dimensional View of Alumina Clusters in Aluminum-Killed Low-Carbon Steel," Met. Trans. AIME, Vol. 1 (9), 1970, 2652.

59.   K. Okohira, N. Sato and H. Mori, "Observation of Three-Dimensional Shapes of Inclusions in Low-Carbon Aluminum-Killed Steel by Scanning Electron Microscope," Trans. ISIJ, Vol. 14, 1974, 103-109.

60. R. Rastogi and A.W. Cramb, "Inclusion Formation and Agglomeration in Aluminum-killed Steels," in 2001 Steelmaking Conference Proceedings, Vol. 84, ISS, Warrendale, (Baltimore, Maryland, USA), 2001, 789-829.

61. M. Olette, "Institut de Recherches de La Siderurgie Francaise," Report, IRSIO, 1972.

62. K. Asano and T. Nakano, "Deoxidation of Molten Steel with Deoxidizer," Trans. ISIJ, Vol. 12, 1972, 343-349.

63. H. Ooi, T. Sekine and G. Kasai, "On the Mechanisms of Alunima Cluster Formation in Molten Iron," Trans. ISIJ, Vol. 15, 1975, 371-379.

64. N. Aritomi and K. Gunji, "Morphology and Formation Mechanism of Dendritic Inclusions in Iron and Iron-Nickel Alloys Deoxidized with Silicon and Solidified Unidirectionally," Trans. ISIJ, Vol. 19, 1979, 152-161.

65. T.B. Braun, J.F. Elliott and M.C. Flemings, "The Clustering of Alumina Inclusions," Metal. Trans. B, Vol. 10B (6), 1979, 171-184.

66. N. Aritomi and K. Gunji, "On the Formation of Dendritic Inclusion from a Spherical Primary Silica in Iron-10% Nickel Alloy Deoxidized with Silicon," Trans. ISIJ, Vol. 20, 1980, 26-32.

67. Y. Miki, H. Kitaoka, T. Sakuraya, T. Fujii, "Mechanism for Separating Inclusions from Molten Steel Stirred with a Rotating Electro-Magnetic Field," ISIJ Inter., Vol. 32 (1), 1992, 142-149.

68. W.K. Tiekink, A. Pieters and J. Hekkema, "Al2O3 in Steel: Morphology Dependent on Treatment," I & Smaker, Vol. 21 (7), 1994, 39-41.

69. T. Murai, H. Matsuno, E. Sakurai, H. Kawashima, "Separation Mechanism of Inclusion from Molten Steel during RH Treatment," Tetsu-to-Hagane, Vol. 84 (1), 1998, 13-18.

70. L. Zhang and S. Taniguchi, "Fluid Flow and Inclusion Removal in Continuous Casting Tundish," Metal. & Material Trans. B., Vol. 31B (2), 2000, 253-266.

71. K. Nakanishi and J. Szekely, "Deoxidation Kinetics in a Turbulent Flow Field," Trans. ISIJ, Vol. 15, 1975, 522-530.

72. L. Kampmann and M. Kahlweit, "On the Theory of Precipitations II," Berichte der Bunsen-Gesellschaft physikalische Chemie, Vol. 74 (5), 1970, 456-462.

73. F. Oeters, Metallurgy of Steelmaking, Verlag Stahleisen mbH, 1994, 347.

74. T. Kawawa and M. Ohkubo, "A Kinetics on Deoxidation of Steel," Trans. ISIJ, Vol. 8, 1968, 203-219.

75. K. Ogawa, "Slag Refining for Production of Clean Steel," in Nishiyama Memorial Seminar, Vol. 143/144, Iron and Steel Institute of Japan, (ISS, Tokyo), 1992, 137-166.

76. M. Matsuno, Y. Kikuchi, M. Komatsu, M. Arai, K. Watanabe, H. Nakashima, "Development of New Deoxidation Technique for RH Degassers," <u>I & Smaker,</u> Vol. 20 (7), 1993, 35-38.

77. D. Reay and G.A. Ratcliff, <u>The Canadian J. of Chem. Eng.,</u> Vol. 51, 1973, 178-185.

78. J.R. Grace, <u>Trans. Inst. Chem. Eng.,</u> Vol. 54, 1976, 167-173.

79. T. Tadaki and S. Maeda, <u>Chemical Engineering (In Japanese),</u> Vol. 25 (4), 1961, 254-264.

80. V.G. Levich, "Physicochemical Hydrodynamics," in <u>Physicochemical Hydrodynamics</u>, Englewood Cliff: Prentice Hall London, 1962, 209,216,224,395-470.

81. F.N. Peebles and H.J. Garber, <u>Chem. Eng. Prog.,</u> Vol. 49, 1953, 88.

82. R. Clift, J.R. Grace and M.E. Weber, <u>Bubbles, Drops and Particles</u>, Academics Press, INC., New York, 1978.

83. R.M. Davies and G. Taylor, <u>Proc. R. Soc. London Ser.,</u> Vol. A200, 1950, 375-390.

84. B.G. Thomas, L.J. Mika and F.M. Najjar, "Simulation of Fluid Flow Inside a Continuous Slab Casting Machine," <u>Metall. Trans. B,</u> Vol. 21B (2), 1990, 387-400.

85. T.C. Hsiao, T. Lehner and B. Kjellberg, <u>Scand. J. Metallurgy,</u> Vol. 8, 1980, 105.

86. M. Sevik and S.H. Park, <u>J. of Fluids Eng. Trans. AIME</u> (53-60), 1973,
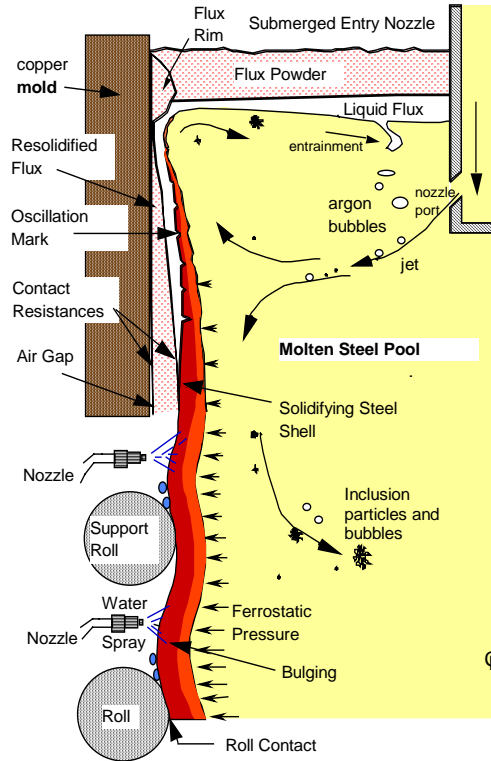
Figure 1. .Schematic of Flow Phenomena in Mold Region of Continuous Casting Process.
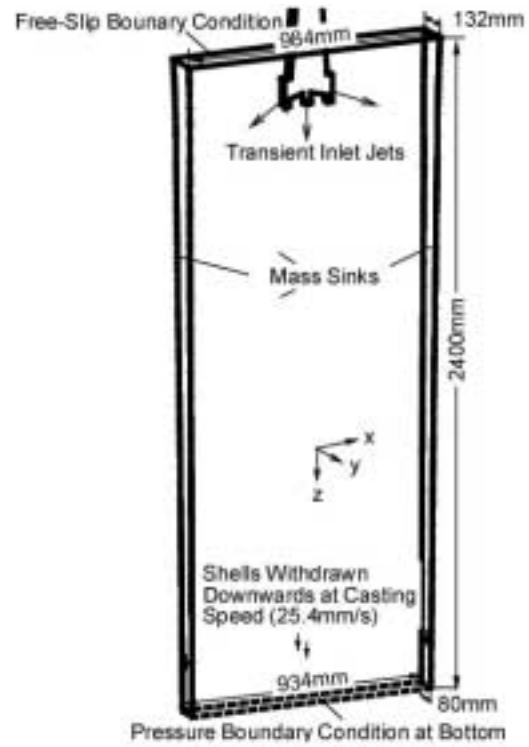
Figure 2. Schematic of the computational domain.

(a)

(b)
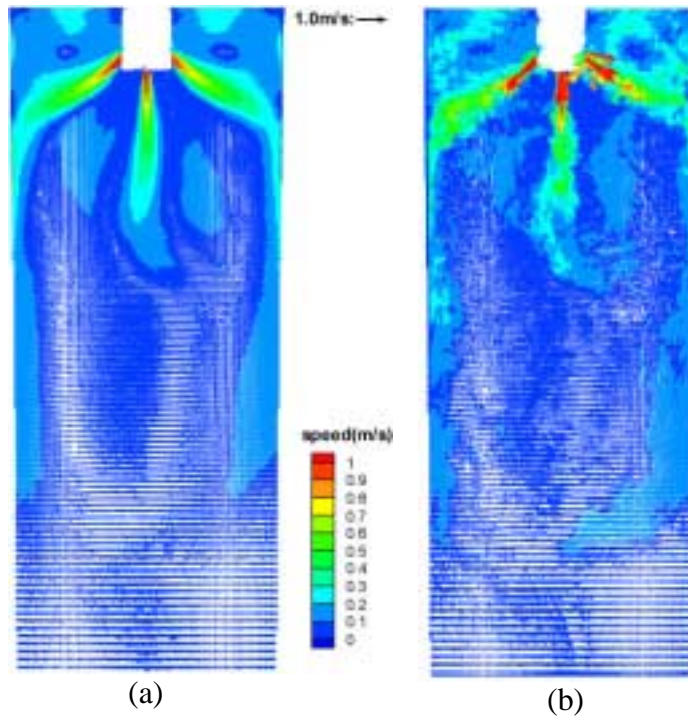
Figure 3. Velocity field at the center plane between wide faces (a) time averaged plot, (b) a typical instantaneous plot.
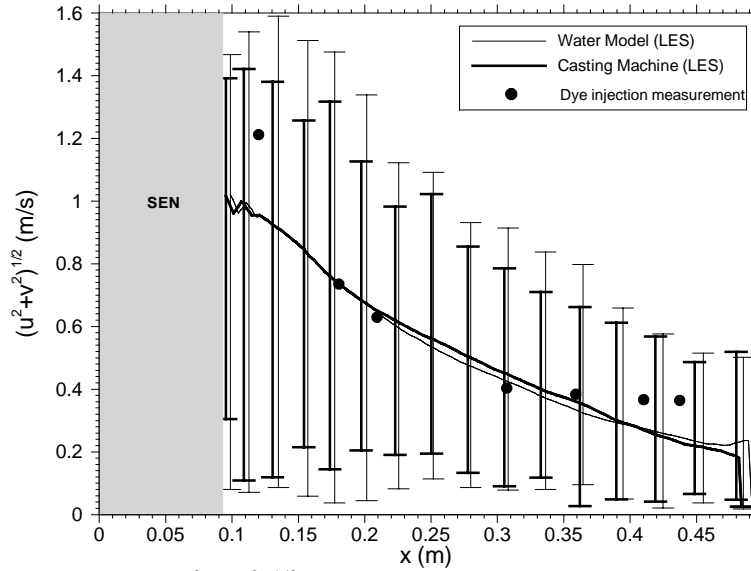
Figure 4. Comparison of $(u^2 + v^2)^{1/2}$ along jet centerline, obtained from LES and dye injection measurements (full-scale water model).
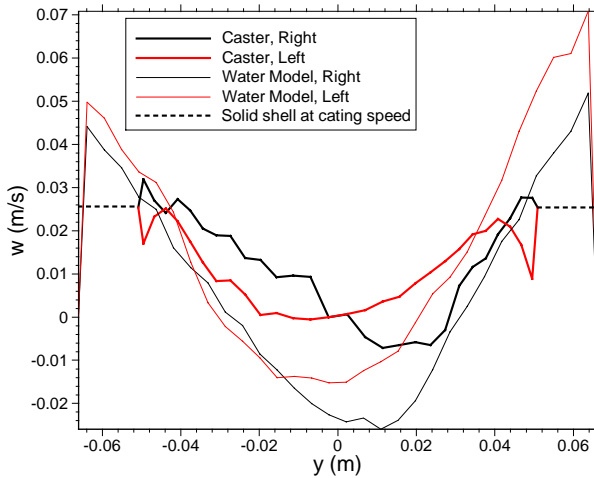
Figure 5. Comparison of downwards velocities of the full scale water and casting machine along a horizontal line.
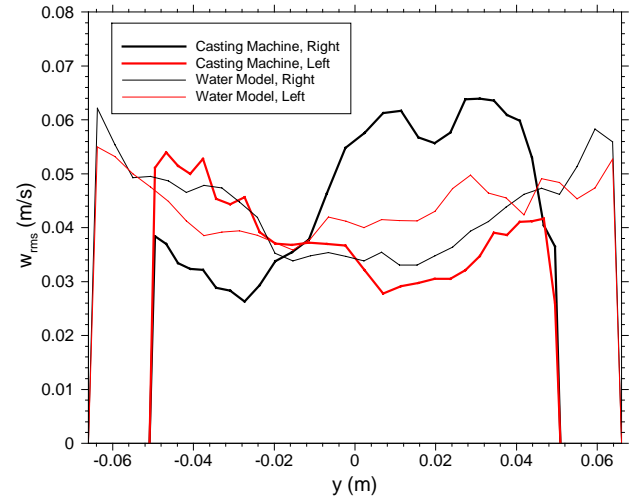
Figure 6. Comparison of *rms* of the downwards velocity of the full scale water and casting machine along a horizontal line.
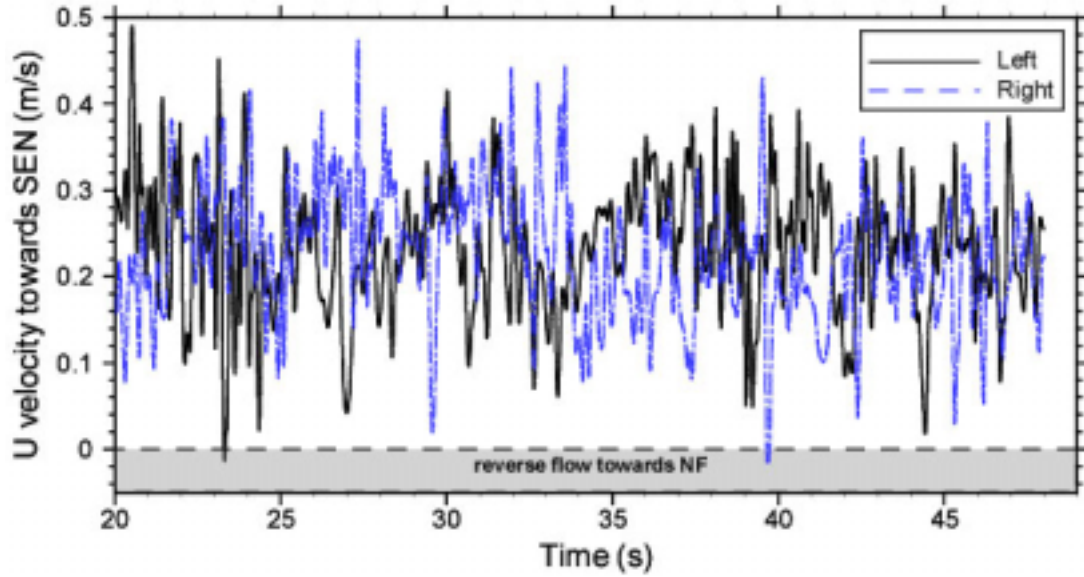
Figure 7. Time variation of horizontal velocity towards SEN at the center points of the two sides of the top surface.
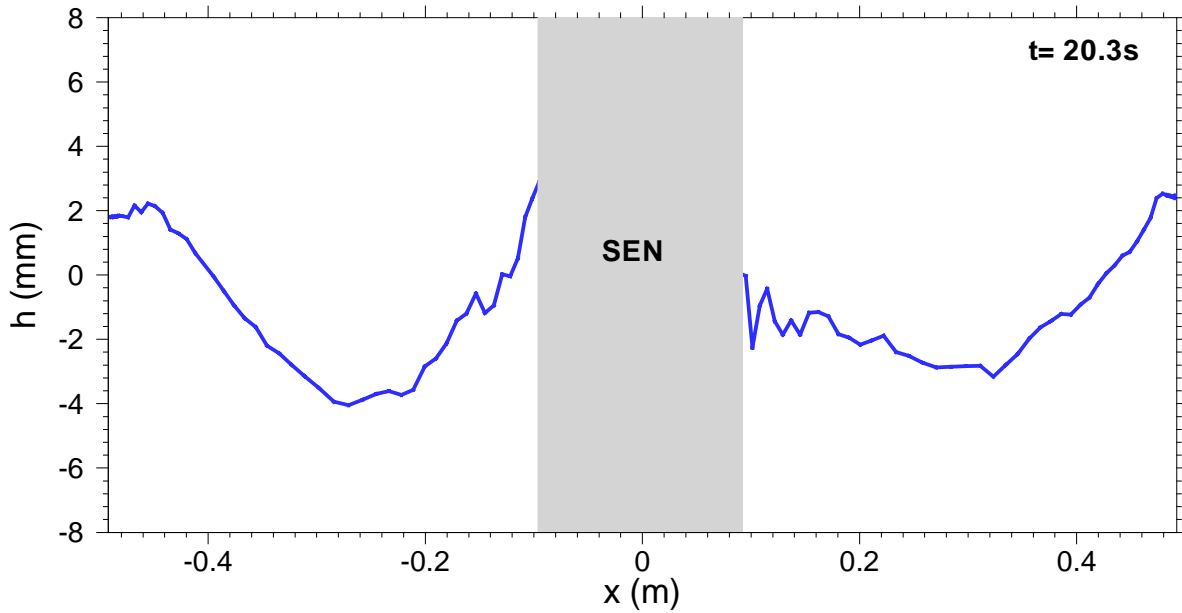
Figure 8. A typical top level fluctuation approximated from the computed pressure by ($\dfrac{(p - p_{mean})}{(\rho_{steel} - \rho_{flux}) g}$), obtained from LES.
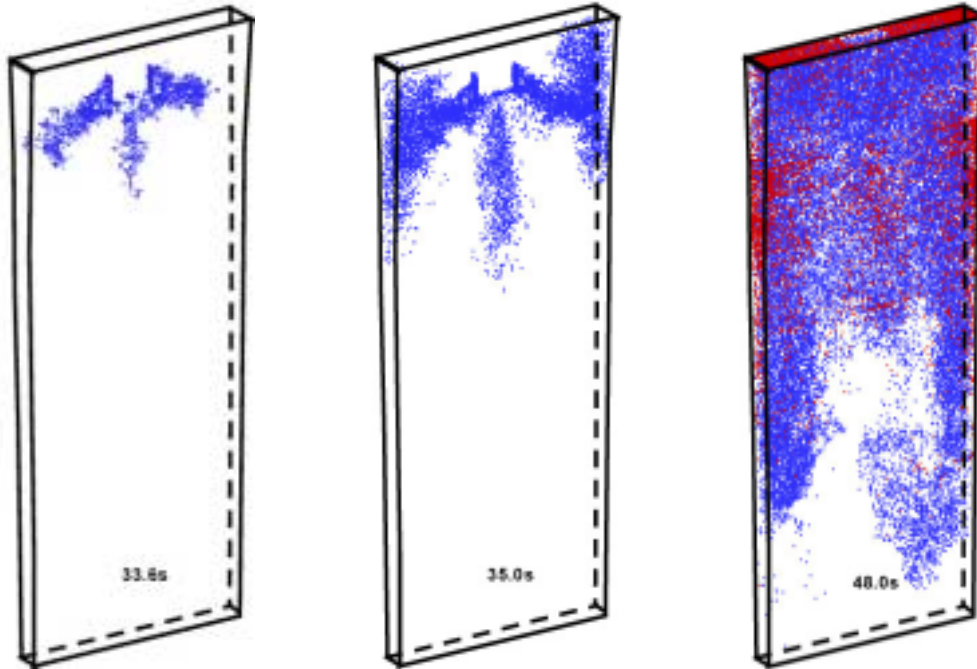
Figure 9. Particle distributions at three instants (blue dots are moving particles; red dots are entrapped particles by solidifying shell).
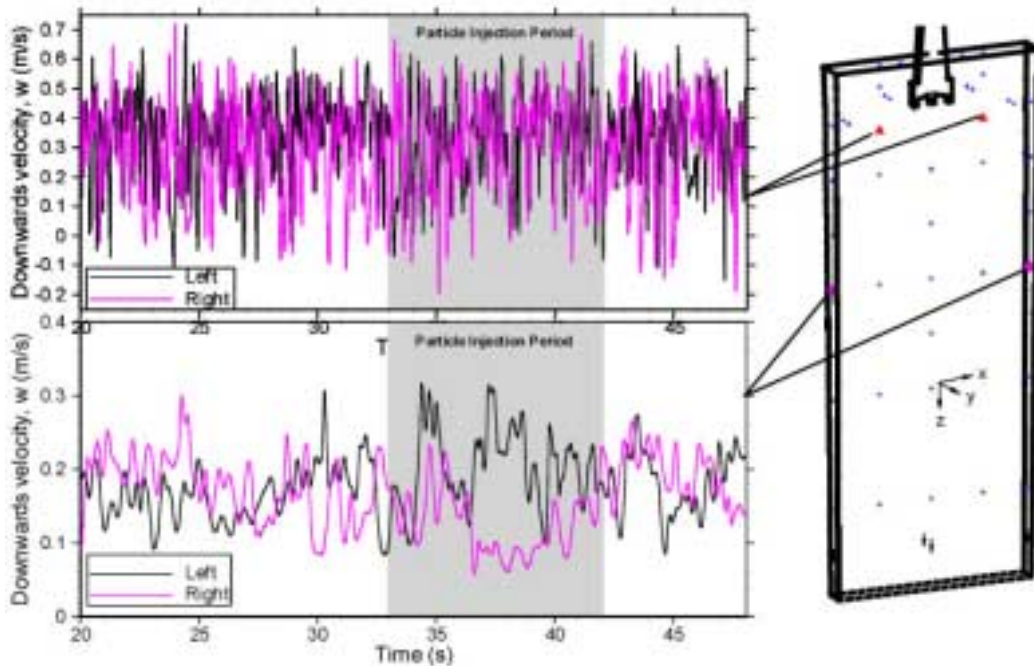
Figure 10. Time variation of downwards velocity at two points showing inherent transient asymmetry of the lower rolls.
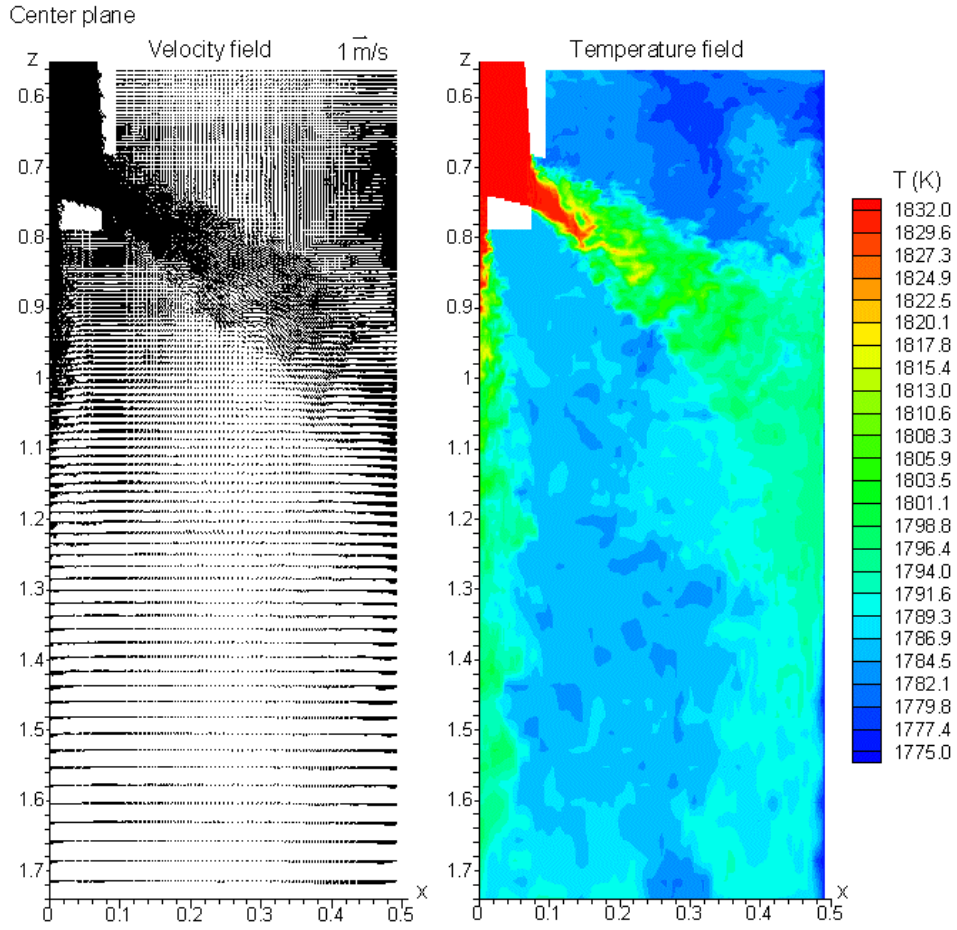
Figure 11. Instantaneous velocity vector (left) and temperature contour (right) plots.
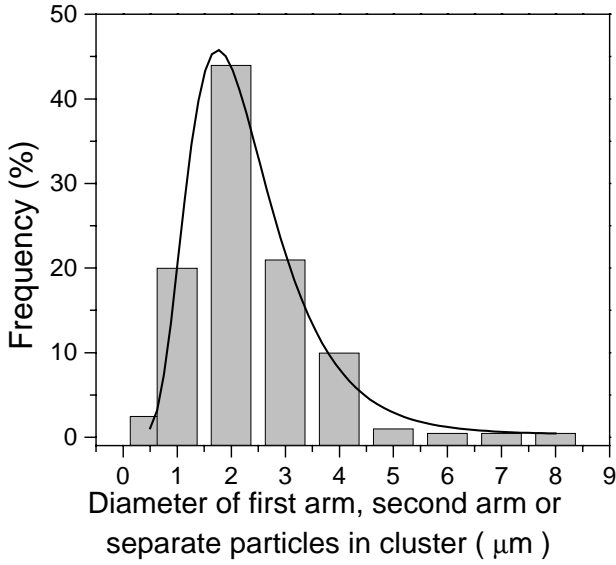
Figure 12. The smallest size feature of alumina inclusions in Steel
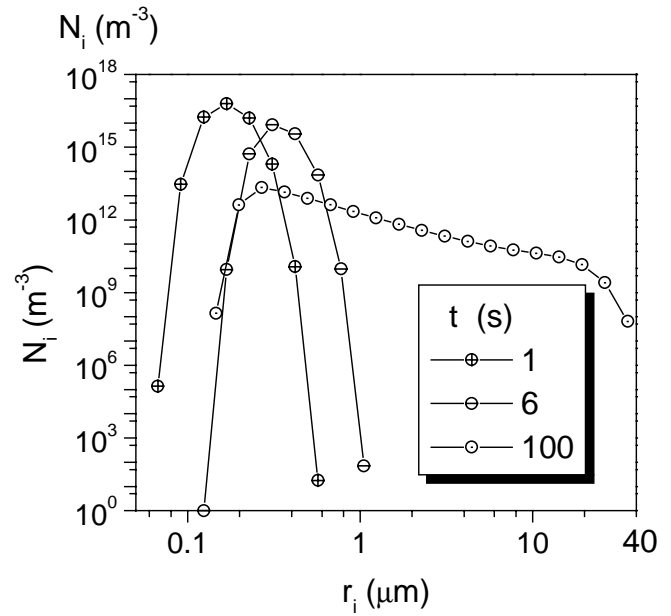
Figure 13. Inclusion size distribution as a function of time
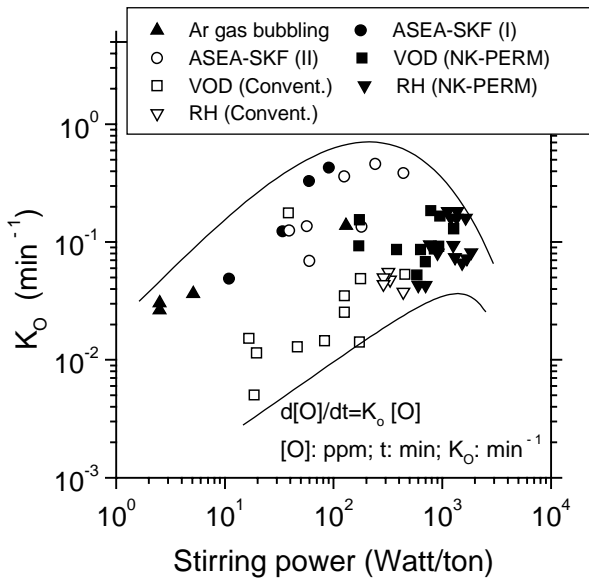
Figure 14. Effect of stirring power on deoxidation rate constant
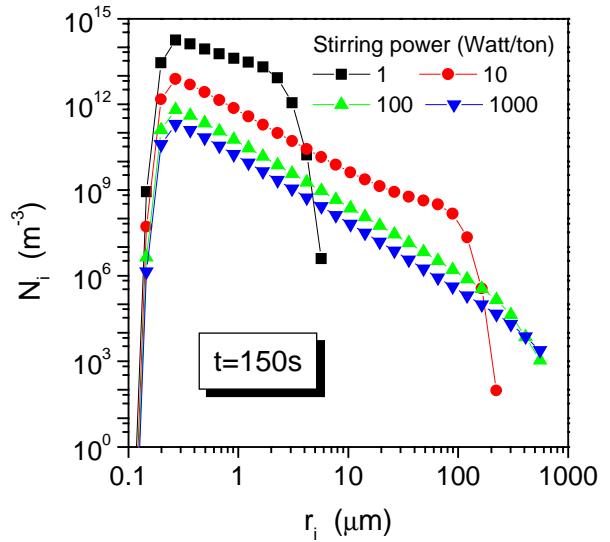
Figure 15. Effect of stirring power on inclusion size distribution
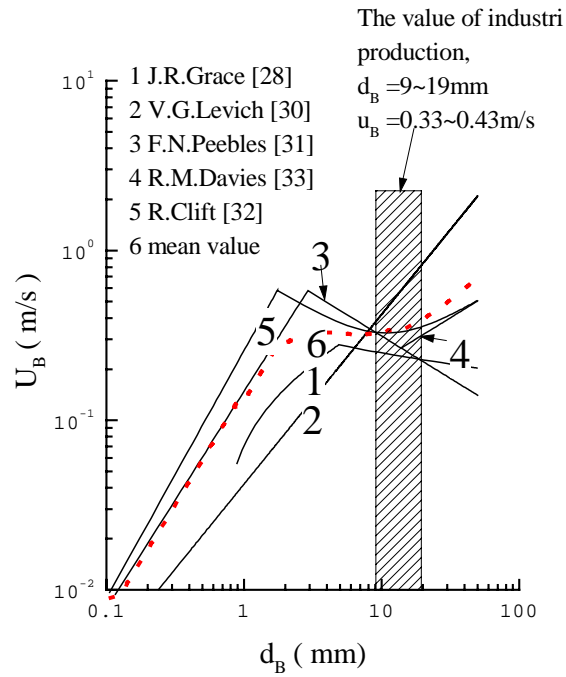
Figure **16.** Terminal velocities of gas bubbles in liquid steel as a function of bubble size
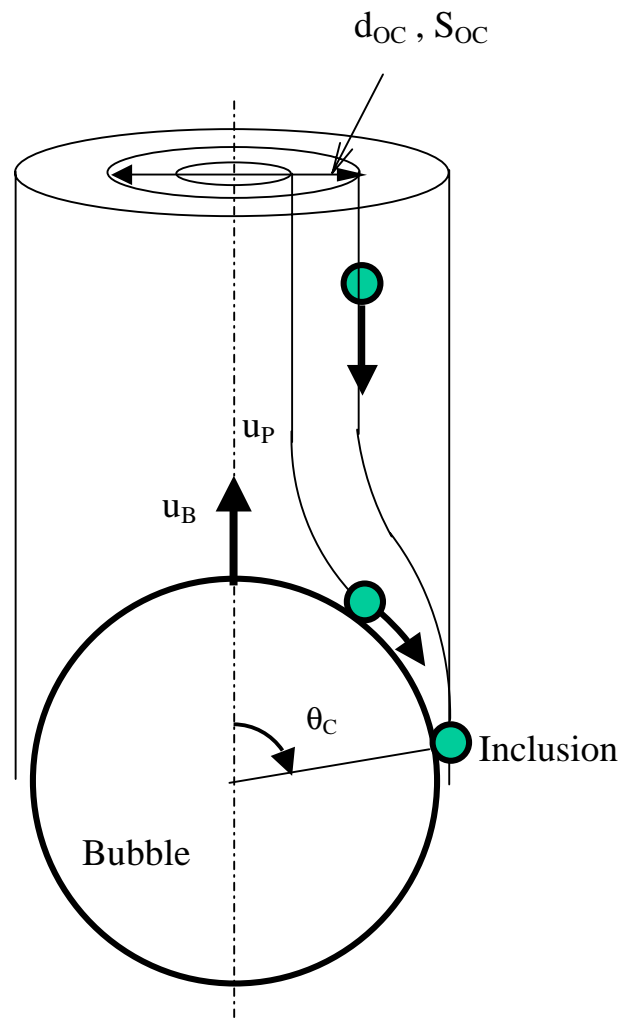
Figure **17.** Schematic of collision and adhesion of inclusions on a bubble
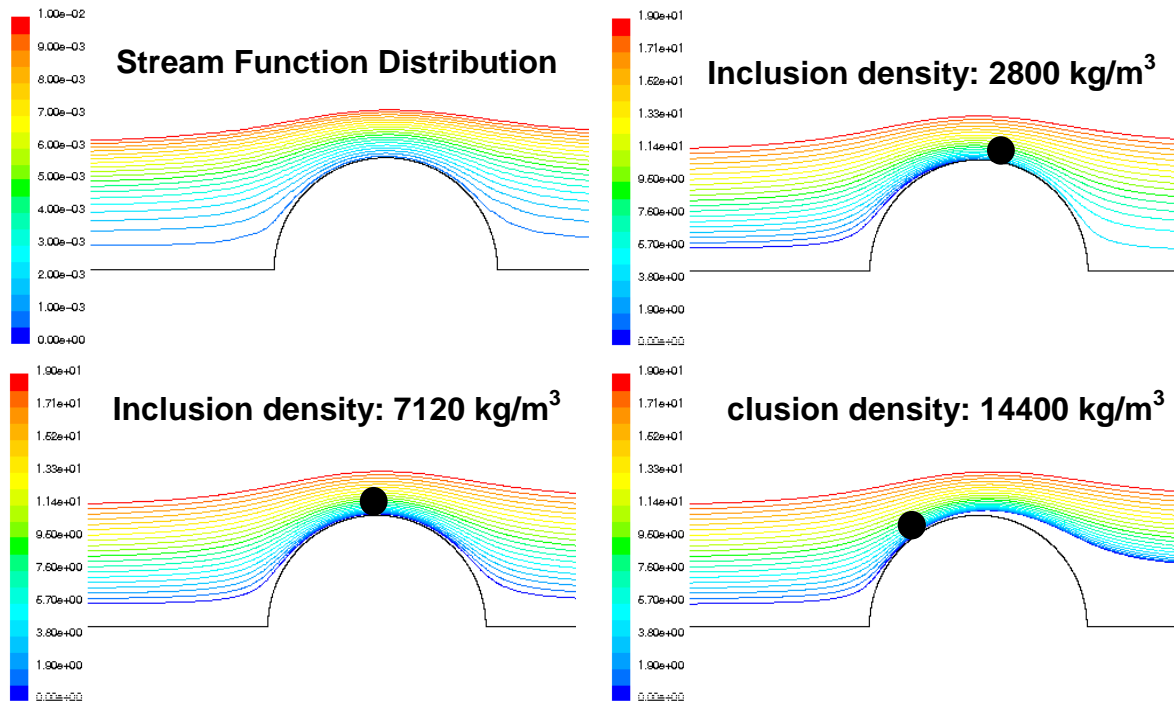
Figure **18.** The trajectory and attachment around a bubble of 100 μm inclusions with different density compared to the streamline distribution
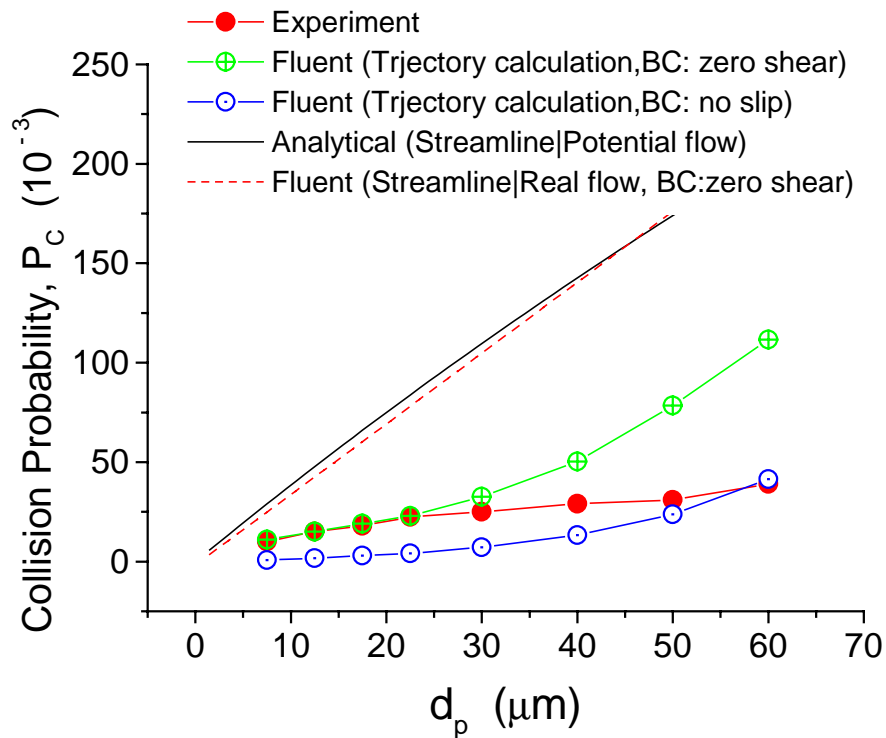
Figure **19.** Comparison of measured probability of collision between silica particles and air bubbles in water with various mathematical models
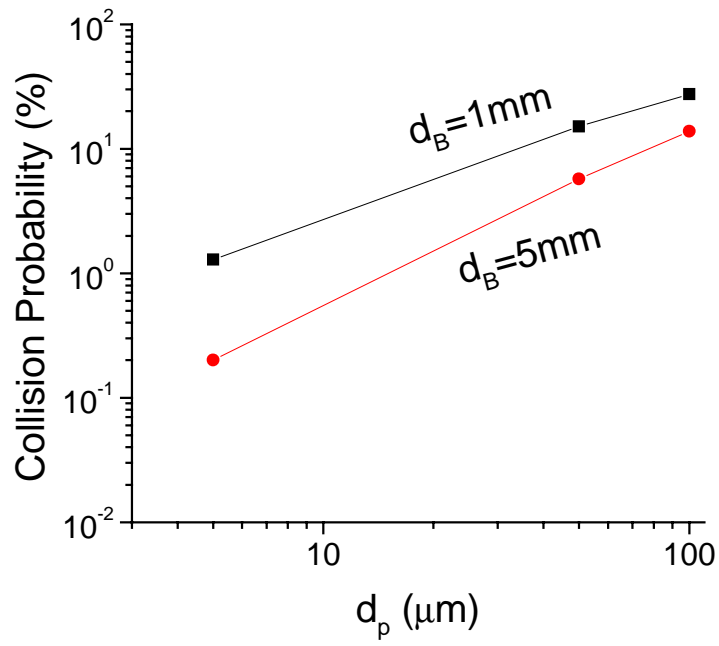
Figure **20.** Collision probabilities calculated between argon bubble and alumina inclusions in liquid steel
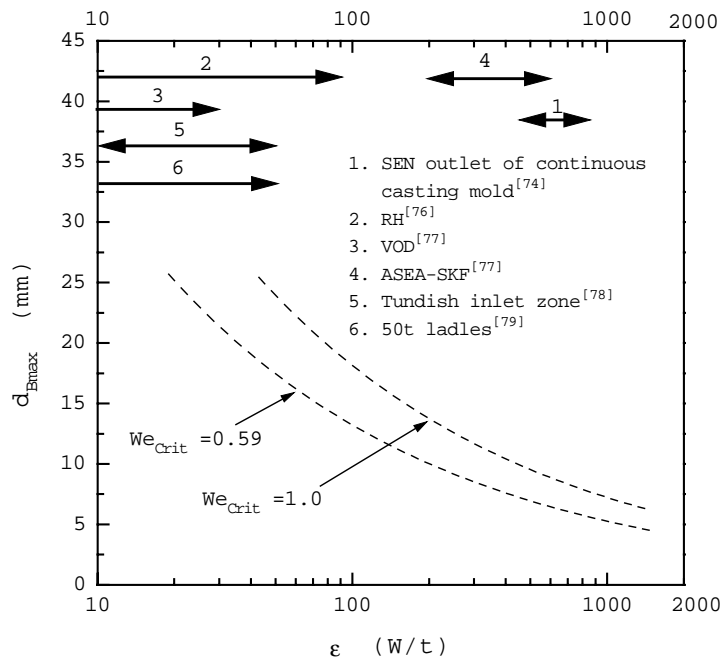
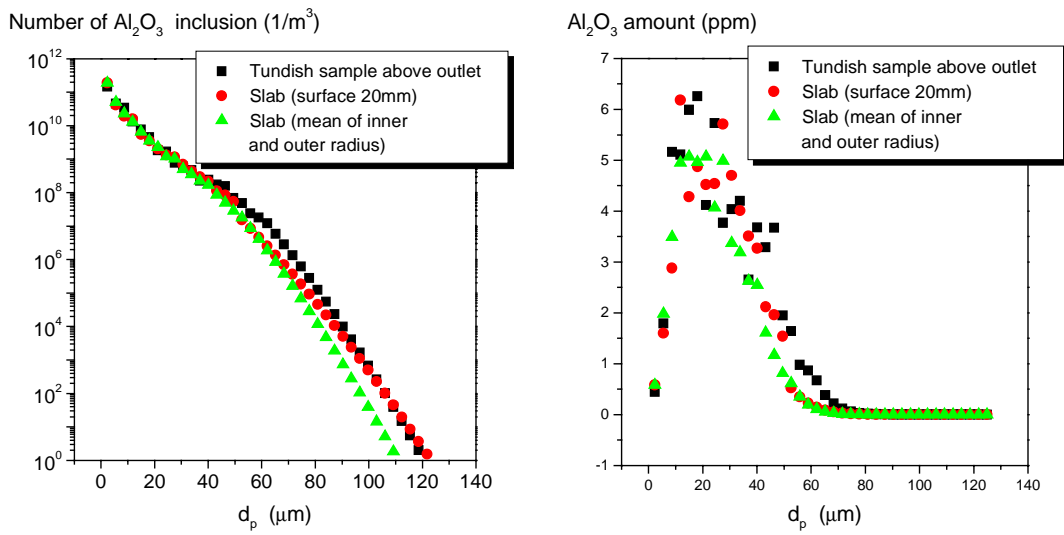Figure **21.** The relationship between the stirring intensity and bubble size

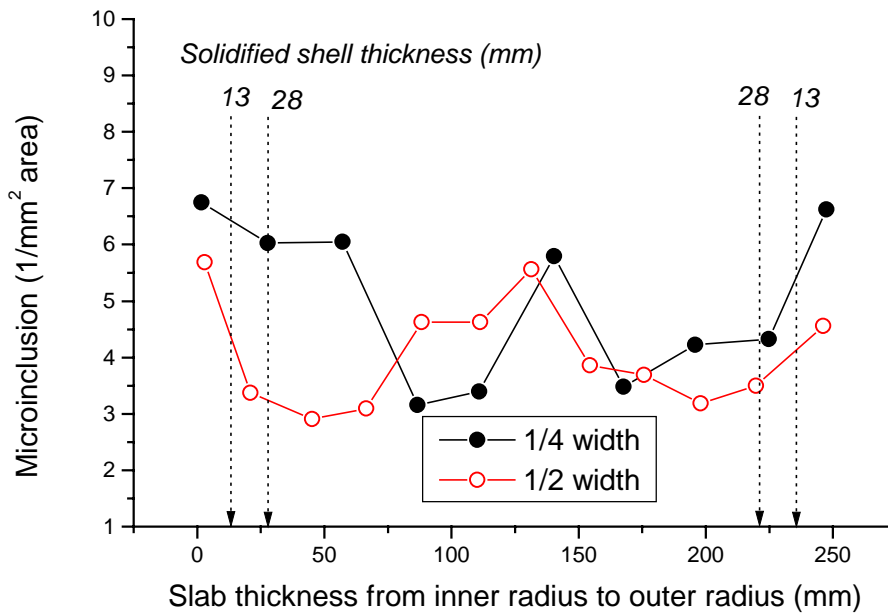Figure **22**. Inclusion size distribution for samples in tundish and slab

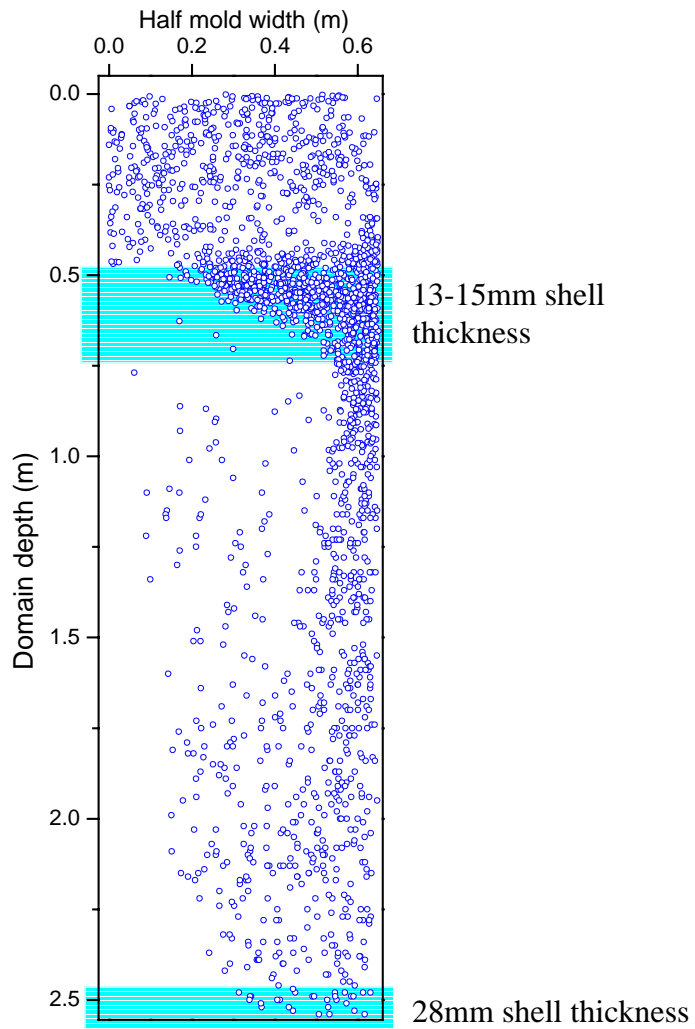Figure **23.** Inclusion distribution along the slab thickness of continuous casting slab

Figure **24.** The simulated entrapped 50 μm inclusion positions on wide face